analytical chemistry

ARTICLE

pubs.acs.org/ac

Analysis of Native Biological Surfaces Using a 100 kV Massive Gold Cluster Source

Francisco A. Fernandez-Lima,[†] Jeremy Post,[‡] John D. DeBord,[†] Michael J. Eller,[†] Stanislav V. Verkhoturov,[†] Serge Della-Negra,[§] Amina S. Woods,[‡] and Emile A. Schweikert*[,†]

[†]Department of Chemistry, Texas A&M University, College Station, Texas 77843-3255, United States

[‡]Structural Biology Unit, NIDA IRP, NIH, Baltimore, Maryland 21224, United States

[§]Institut de Physique Nucléarie d'Orsay, 91406 Orsay, France

ABSTRACT: In the present work, the advantages of a new, 100 kV platform equipped with a massive gold cluster source for the analysis of native biological surfaces are shown. Inspection of the molecular ion emission as a function of projectile size demonstrates a secondary ion yield increase of ~100× for 520 keV Au_{400}^{4+} as compared to 130 keV Au_3^{1+} and 43 keV C_{60}. In particular, yields of tens of percent of molecular ions per projectile impact for the most abundant components can be observed with the 520 keV Au_{400}^{4+} probe. A comparison between 520 keV Au_{400}^{4+} time-of-flight-secondary ion mass spectrometry (TOF-SIMS) and matrix assisted laser desorption ionization-mass spectrometry (MALDI-MS) data showed a similar pattern and similar relative intensities of lipid components across a rat brain sagittal section. The abundant secondary ion yield of analyte-specific ions makes 520 keV Au_{400}^{4+} projectiles an attractive probe for submicrometer molecular mapping of native surfaces.

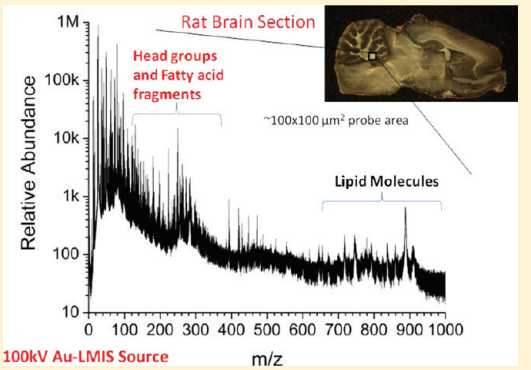

Mass spectrometry imaging has become the method of choice for chemical mapping of organic and inorganic compounds from various surfaces, in particular for tissue sections (for more details see reviews 1−5). Three techniques are emerging as good candidates: MALDI-MS, nano-SIMS, and TOF-SIMS. In MALDI-MS, molecular ion identification and localization with a 50 μm spatial and nanomolar sensitivity can be achieved over a wide mass range (typically, 400−40 kDa), while analysis reproducibility depends strongly on the sample preparation method and matrix deposition. That is, the matrix remains a crucial choice for the chemical class to be studied in MALDI experiments and a number of new matrixes have been developed (e.g., ionic liquids,[6] nanoparticules,[7,8] colloids,[9] implantation of absorption sites,[10] and engineered organic matrixes[11−14] for lipid analyses).

Nano-SIMS and TOF-SIMS, on the other hand, are perfectly suited for high spatial resolution and have the unique advantage that analysis can be performed on native surfaces. In the case of nano-SIMS, a very precise localization of elements or small fragments within a few tens of nanometers is achievable. This mass range limitation requires strategies for molecular identification (e.g., isotopic labeling) which can limit their applicability.[15]

TOF-SIMS can detect molecular ions with a spatial resolution of 500 nm to a few micrometers. The selection of the primary ion in a TOF-SIMS experiment defines the mass range of the analysis. For example, monatomic projectiles (e.g., In, Ga, and Cs ion sources) induce high surface damage and low intact molecular ion emission, leading mainly to the detection of fragment ions (e.g., head groups in the case of lipid samples).[16] When small cluster ion sources (e.g., Au_3^+ and Bi_3^+) are used,[17,18] TOF-SIMS can also generate molecular signals in the 1000−1500 mass range. Moreover, the use of larger cluster projectiles (e.g., C_{60} and Au_{400}) with TOF-SIMS for surface analysis and characterization has shown significant advantages due to the enhanced emission of molecular ions and reduced molecular fragmentation.[19−22] With temporally and spatially discrete cluster impacts, the small interaction volume (~10^3 nm^3) and large ionized ejecta makes these massive probes promising candidates for surface molecule interrogation.[23,24] Current challenges are in the development of new TOF-SIMS probes capable of generating signature secondary ions from a surface of interest. Recent efforts have focused on the use of higher energy and larger cluster projectiles (e.g., C_{60} and Au_{400}) to increase the secondary ion signal.[25−28]

In the present paper, we introduce a massive gold projectile source installed in a new, 100 kV platform as a new generation TOF-SIMS probe for the analysis of native biological surfaces. Molecular ion emission profiles are compared with MALDI imaging data for model rat brain sagittal sections. In particular, secondary ion dependence on the projectile size and the advantages of 520 keV Au_{400}^{4+} single impacts will be shown for surface molecule characterization and identification on native, rat brain sagittal sections.

Received: June 14, 2011
Accepted: October 3, 2011
Published: October 03, 2011

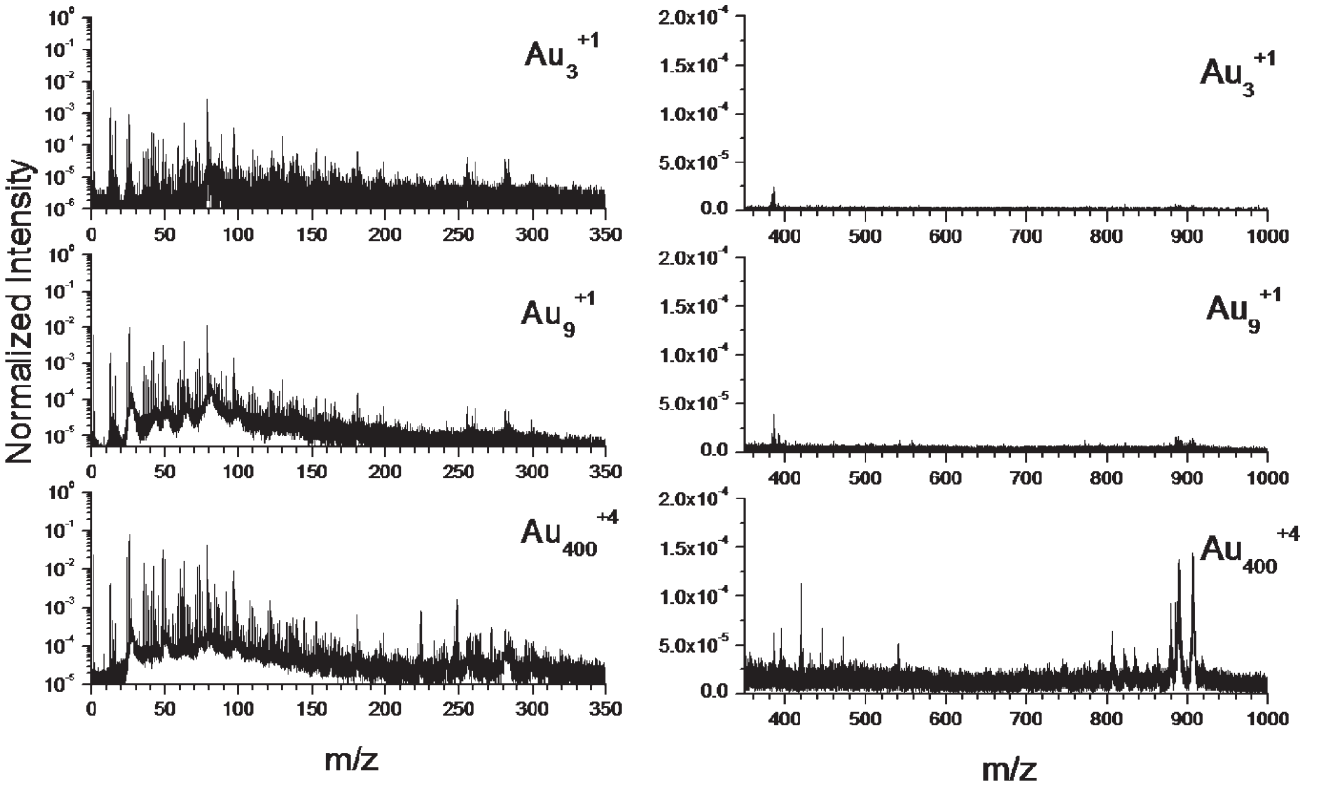

Figure 1. Representative negative ion mode single event TOF-SIMS spectra for 130 keV Au_3^{1+}, 130 keV Au_9^{1+}, and 520 keV Au_{400}^{4+} projectiles on a native rat brain section from the same 100 × 100 μm^2 field of view. All spectra are normalized to the number of impacts (typically 10^6 impacts). Notice the increase in molecular ion emission for the massive cluster projectile.

EXPERIMETAL METHODS

Cluster-SIMS Experiments. A new, in-house built experimental setup comprising a massive gold cluster primary ion beam, an electron emission microscope, and a TOF mass spectrometer have been developed. The gold cluster primary ion beam consists of a Au-liquid metal ion source (Au-LMIS) coupled to a 100 kV Pegase platform.[29] The Au-LMIS is floated to 20 kV relative to the Pegase platform and can produce a variety of projectiles, ranging from atomic $Au_1^{1,2+}$ to polyatomic Au_{2-9}^{1+} to massive Au_{100n}^{+n} clusters; more details on the primary ion distribution produce by the Au-LMIS can be found in ref 30. The primary ion projectiles can be mass-selected using a Wien filter and focused into the analysis chamber, where the primary ion current can be measured as a function of the projectile size (e.g., 150 nA for Au_1^+, 15 nA for Au_3^+, and 1 nA for Au_{400}^{4+} without beam collimation/pulsing). Comparative studies were performed using a C_{60} in-house built ion source capable of producing 15−43 keV C_{60} ions; details of the C_{60} effusion source can be found elsewhere.[31]

All TOF-SIMS experiments were performed under single projectile impacts. To achieve the single impact analysis mode, the primary ion beam was pulsed and/or collimated to ensure an impact rate below 500 Hz of individual projectiles per pulse. All experiments were performed in negative ion mode and the target was set to −10 kV; under these conditions the primary ions experienced a total acceleration of 130 kV. Emitted electrons and negative secondary ions were collected per single projectile impact. Emitted electrons were accelerated from the target and then deflected using a weak magnetic field toward an electron emission microscope and used as a TOF start signal (negative ion mode detection).[31] Secondary ions were accelerated and analyzed using an in-house built TOF analyzer (∼1.7 m long) equipped with a two-stage electrostatic mirror (mass resolution of ∼1000−1500). TOF signals of the secondary ions were detected using a newly designed, pie-shaped eight-anode detector and were stored on a multichannel time-to-digital converter (TDC). The multianode detector guarantees detection of high multiplicity secondary ions (up to eight isobaric ions). New data acquisition and processing programs (SAMPI) were developed in-house to optimize multiple secondary ion detection.

MALDI Imaging Experiments. MALDI imaging experiments were performed using a nitrogen laser (337 nm) in a commercial LTQ-XL instrument (Thermo Fisher Scientific Inc., Santa Clara, CA). Data were acquired in negative ion mode from a sagittal brain section (∼12 mm × 25 mm) with a pixel resolution of 100 × 100 μm^2. A saturated matrix solution of 2,6-dihydroxyacetophenone [DHA]/ammonium sulfate 125 mM/heptafluorobutyric acid [HFBA] 0.05% was used (more details in refs 14 and 32). Matrix solution (∼2.5 mL) was sprayed on the tissue section with an artistic brush (Aztek A470/80 Airbrush system, Testor Corporation, Rockford, IL).[33] To ensure sufficient evaporation of organic solvents, 2 min intervals between spray cycles were used. The spray nozzle was positioned 15−20 cm from the sample plate, and matrix was sprayed at a temperature of ∼4−10 °C.

Sample Preparation. Details of sample preparation can be found elsewhere.[34] Briefly, Male Sprague- Dawley rats (Harlan Industries, Indianapolis, IN) between 300 and 420 g were euthanized with isoflurane and the brain quickly removed and

Table 1. Secondary Ion Yields Per Nominal Mass of Representative Signals As a Function of the Projectile Size from Single Event TOF-SIMS Analysis on Native Rat Brain Sections

secondary ion	(m/z)	130 keV Au_3^+	130 keV Au_9^+	43 keV C_{60}^{+2}	520 keV Au_{400}^{+4}
CN^-	26	2.79×10^{-2}	3.75×10^{-1}	1.12×10^{-1}	3.56
PO_2^-	63	4.21×10^{-2}	2.25×10^{-1}	9.48×10^{-2}	8.64×10^{-1}
PO_3^-	79	2.60×10^{-1}	8.10×10^{-1}	2.75×10^{-1}	3.02
Au^-	197	4.71×10^{-3}	9.43×10^{-3}		5.65×10^{-2}
$Au(CN)^-$	223				3.78×10^{-2}
$Au(CN)_2^-$	249				1.47×10^{-1}
ST 22:0 (OH)	878.6	2.65×10^{-4}	9.01×10^{-4}	5.07×10^{-4}	1.49×10^{-2}
PI 38:4	885.5	7.31×10^{-4}	2.35×10^{-3}	1.02×10^{-3}	1.50×10^{-2}
ST 24:1	888.7	1.01×10^{-3}	2.46×10^{-3}	7.97×10^{-4}	3.11×10^{-2}
ST 24:0	890.6	9.63×10^{-4}	2.32×10^{-3}	8.35×10^{-4}	2.82×10^{-2}
ST 24:1 (OH)	904.6	6.44×10^{-4}	1.63×10^{-3}	7.92×10^{-4}	2.53×10^{-2}
ST 24:0 (OH)	906.6	7.76×10^{-4}	2.26×10^{-3}	9.63×10^{-4}	3.42×10^{-2}

frozen in isopentane for 15 s, prior to storage at −80 °C. Before sectioning, brains were allowed to reach a temperature of −20 °C for 45 min in the cryostat chamber (CM 3050 S, Leica Microsystem Nussloch, Germany). The brain was attached to the cryostat specimen disk using ice slush made from distilled water.[33] Brain sagittal sections 10 μm thick were cut and placed on a stainless steel support. Two consecutive sections were used for the TOF-SIMS and MALDI imaging.

RESULTS AND DISCUSSION

Previous studies have shown that secondary ion emission in TOF-SIMS depends strongly on the projectile size and energy.[35,36] For example, from model organic samples, the secondary ion emission for small gold projectiles (e.g., Au_3) reaches a maximum around 30−40 keV/atom.[27] Figure 1 shows representative TOF-SIMS spectra for 130 keV Au_3^{1+}, 130 keV Au_9^{1+}, and 520 keV Au_{400}^{4+} single impacts on the same region of a native, rat brain sagittal section (~100 × 100 μm^2 field of view). Inspection of Figure 1 shows that although similar in the low mass region, there is a strong increase in the molecular ion signal as the projectile size increases.

For a more detailed inspection, secondary ion yields (number of molecular ions detected per projectile impact) are reported in Table 1. Multiple isobaric atomic and small fragment ions are observed per projectile impact for the case of 520 keV Au_{400}^{4+}. In the low mass region, similar MS signals are observed with the exception of gold adduct signals in the case of 520 keV Au_{400}^{4+} (e.g., $AuCN^-$ and $Au(CN)_2^-$), as characteristic signatures of the massive projectile−target interaction.[37] In the case of molecular ion emission, inspection shows that 520 keV Au_{400}^{4+} secondary ion yields are ~10× and ~30−80× higher when compared to 130 keV Au_9^{1+} and 130 keV Au_3^{1+}, respectively. Comparison with 43 keV C_{60} projectiles shows that the secondary ion yields lie between those obtained with 130 keV Au_3^{1+} and Au_9^{1+} projectiles and are ~30× smaller than those obtained with 520 keV Au_{400}^{4+} projectiles.

Three ion distributions are observed for TOF-SIMS with single 520 keV Au_{400}^{4+} impacts (i) headgroup fragments, (ii) fatty acid fragments, and (iii) lipid molecular ions. We attribute the high abundance of lipid secondary ion signal as compared to other chemical classes to the fact that lipids account for up to 50%

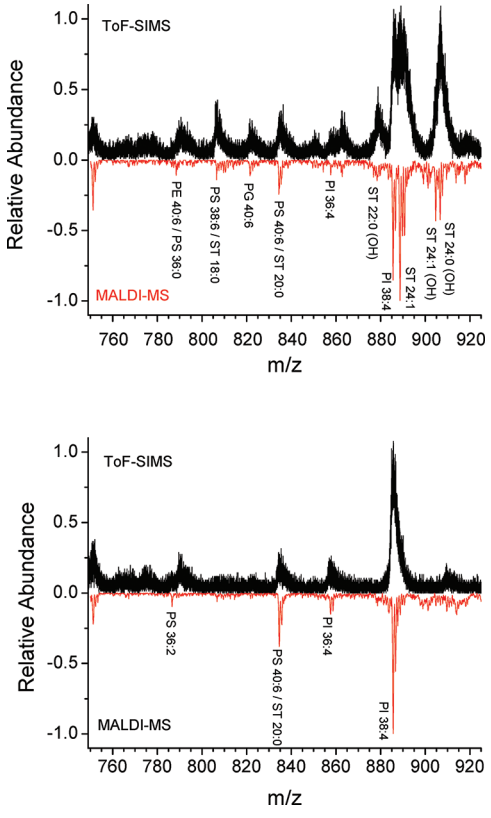

Figure 2. Representative 520 keV Au_{400}^{4+} TOF-SIMS and MALDI-MS spectra of (top) the gray and white matter interface and (bottom) the gray matter regions. In all cases, spectra correspond to a ~100 × 100 μm^2 field of view.

of the dried weight of rat brain tissue sections. During 520 keV Au_{400}^{4+} TOF-SIMS analysis, preferential emission of a particular chemical class is not observed. For example, 0.1−0.5 molecular ions per projectile impact can be obtained with 520 keV Au_{400}^{4+} projectiles from model, single component peptide and lipid targets,[38] where molecular ion abundance is a consequence of the ionization probability and the concentration in the sample.

A complete identification of the lipid signal was performed using a combined TOF-SIMS and MALDI imaging strategy.

dx.doi.org/10.1021/ac201481r |Anal. Chem. 2011, 83, 8448–8453

Table 2. Lipid Species Identified in Negative Ion Mode from 520 keV Au_{400}^{4+} TOF-SIMS and MALDI-MS[a]

Species	Theoretical m/z	ToF-SIMS m/z	MALDI-MS m/z
PE 38:6 / PS 34:0	762.51 / 762.53	762.3	762.53
PE 40:6	774.54	774.4	774.55
PS 36:2	786.53	786.5	786.55
PE 40:6 / PS 36:0	790.54 / 790.56	790.5	790.55
PS 38:6 / ST 18:0	806.50 / 806.55	806.4	806.81
PG 40:6	821.53	821.5	821.83
ST 18:0 (OH)	822.54	822.5	822.69
PS 40:6 / ST 20:0	834.53 / 834.58	834.4	834.58
PI 36:4	857.52	857.5	857.57
ST 22:0 (OH)	878.60	878.5	878.64
PI 38:4	885.55	885.5	885.66
ST 24:1	888.62	888.4	888.65
ST 24:0	890.64	890.6	890.70
ST 24:1 (OH)	904.62	904.5	904.67
ST 24:0 (OH)	906.63	906.5	906.65

[a] In red and blue are denoted lipid signals that are mostly observed in the white and gray matter, respectively.

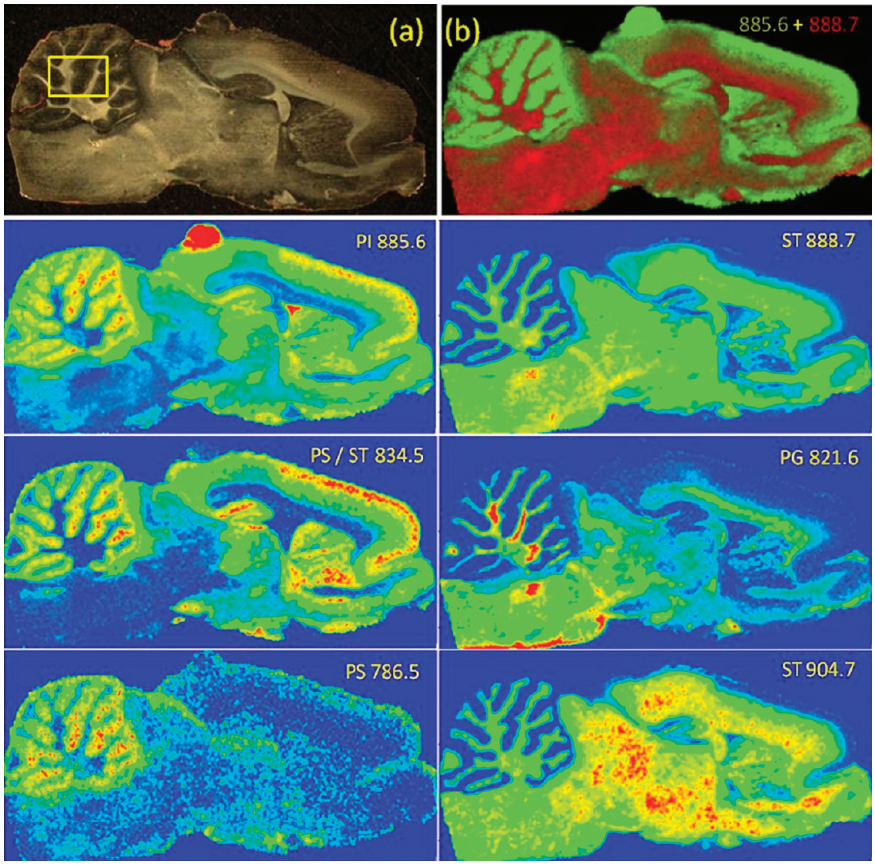

Figure 3. Molecular ion distributions (MALDI-MS) of representative lipid signals in the rat brain slice obtained with 100 × 100 μm^2 pixel resolution. (a) Whole sagittal section optical image and (b) PI (885.6) and ST (888.7) signal overlay. On left and right columns are shown the most abundant lipids observed in the gray and white matter, respectively.

Peak assignment was performed using the MALDI imaging data obtained from a consecutive rat brain sagittal section. For simplicity, here we limit the discussion to the gray and white matter regions of the rat brain cerebellum area. Representative 520 keV Au_{400}^{4+} TOF-SIMS and MALDI-MS spectra of the white and gray region are shown in Figure 2 for equivalent areas (~100 × 100 μm^2 field of view). Inspection of Figure 2 shows that the most abundant signals observed in TOF-SIMS and MALDI-MS are in good correspondence for both the white and gray matter regions; that is, the same lipid pattern is observed in both cases. The reduction in mass resolution observed in the TOF-SIMS spectra is related to the secondary ion focusing

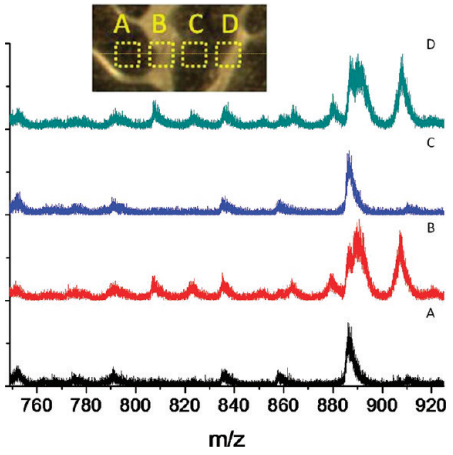

Figure 4. Representative 520 keV Au_{400}^{4+} TOF-SIMS negative ion mode spectra from a line scan A—D across the cerebellum region (top inset, boxes not to scale) of the box highlighted in Figure 3a. All spectra correspond to a 100 × 100 μm^2 field of view and 10^6 impacts.

strategy used to maximize multiple ion detection and transmission; in the single impact TOF-SIMS mode, surface charging is significantly reduced and has a minor effect on the mass resolution. A detailed list of the identified lipids is given in Table 2. It should be noted that for some mass peaks more than one lipid species is possible and assignment was made following MS/MS of the most abundant ones.[39] In the gray matter region, the lipid distribution mainly contains phosphatidylserines (PS) and phosphatidylinotisols (PI). Moreover, the white matter region mainly contains phosphatidylserines (PS), phosphatidylglycerols (PG), and sulfatides (ST).

It is well know that lipids have a wide variety of biological functions. They are the major structural components of cell membranes and are also involved in energy storage and cell-signaling and can function as antioxidants. Each cell type and physiological state of a cell population exhibits a different lipid composition and distribution. This is illustrated in Figure 3 for the whole rat brain sagittal section. A comparison with the optical image (Figure 3a) shows that lipids are distributed across the whole brain section according to tissue composition. For example, Figure 3b shows the complementary distribution of PI 38:4 (gray matter) and ST 24:1 (white matter) in the cerebellum.

A TOF-SIMS line scan across the cerebellum is shown in Figure 4. Inspection of Figure 4 shows that, from A to D, the lipids relative abundances in the white and gray matter vary in good agreement with the MALDI molecular ion distribution shown in Figure 3. ST 24:1, ST 24:1 (OH) and ST 24:0 (OH) are lipids found in the white matter and are abundant in the B and D regions, and are absent in the A and C regions. Since the B and D regions contain some gray matter, PI 38:4 a lipid commonly seen in gray matter only changes in relative abundances. The signal intensity can be further correlated with the surface density of analyte-specific signals; that is, the larger the signal (secondary ion yield) the larger the surface coverage.

It is worth mentioning that in single event 520 keV Au_{400}^{4+} TOF-SIMS, the analytical information comes from the top 10 nm and the surface area interrogated over the whole analysis is less than 1% for a field of view of 100 × 100 μm^2 with 10^6 impacts (assuming an area of emission of 10^2 nm^2 per impact); under these conditions, the surface integrity is preserved (i.e., nondestructive analysis) and no preparation is required. Further applications may include the generation of molecular ion maps from adjacent areas using a movable/automated sample stage, analogous to the MALDI imaging acquisition protocol. On the other hand, preliminary results suggest that Au_{400}^{4+} projectiles can be focused to a 10 × 10 μm^2 field of view which would permit ~100% surface interrogation over the same analysis time (~10^6 impacts).[29]

CONCLUSIONS

In the present study, we have shown the advantages of using high energy, massive gold projectiles for characterization of native biological surfaces. As the projectile's size/energy increases, there is an increase in the secondary ion emission of fragment molecular ions (e.g., head groups and fatty acids for the lipid components). However, the most significant feature is the large increase in the emission yield of lipid molecular ions. For example, a near two order increase in molecular ion yield is obtained with 520 keV Au_{400}^{4+} projectiles compared to 130 keV Au_3^{1+} and 43 keV C_{60} projectiles. The comparison of TOF-SIMS and MALDI-MS secondary ion signals from rat brain sagittal sections shows that a good correspondence for the most abundant target components is observed. In particular, identification of lipid molecular ions can be performed for a field of view of 100 × 100 μm^2 with ~10^6 impacts of 520 keV Au_{400}^{4+}.

The abundant secondary ion yields of analyte-specific ions makes 520 keV Au_{400}^{4+} projectiles an attractive probe for sub-μm molecular mapping of native surfaces. The temporally and spatially discrete single impacts can be used to localize successive stochastic impacts on a ~10 μm diameter spot via the coordinates of the coemitted electrons and hence construct a molecular ion map.[30] The ultimate limits for spatially resolved molecular maps will be set by the number of SIs and electrons ejected per impact (Poisson probability distributions). These as well as steps to enhance mass resolution remain to be explored.

AUTHOR INFORMATION

Corresponding Author

*Address: Department of Chemistry, Texas A&M University, 3255 TAMU, College Station, Texas 77842-3012, United States. Phone: (979) 845-2341. Fax: (979) 845-1655. E-mail: schweikert@chem.tamu.edu.

ACKNOWLEDGMENT

This work was supported by the National Science Foundation (Grant CHE-0750377). F.A.F.-L. acknowledges the National Institute of Health support (Grant No. 1K99RR030188-01)

REFERENCES

(1) Chaurand, P.; Schwartz, S. A.; Reyzer, M. L.; Caprioli, R. M. *Toxicol. Pathol.* **2005**, *33*, 92.

(2) Zimmerman, T. A.; Monroe, E. B.; Tucker, K. R.; Rubakhin, S. S.; Sweedler, J. V. In *Methods in Cell Biology*; Correia, J. J., Detrich, H. W.III, Eds.; Academic Press: San Diego, CA, 2008; Vol. 89, p 361.

(3) Schwartz, S. A.; Caprioli, R. M. *Methods Mol. Biol.* **2010**, *656*, 3.

(4) Amstalden van Hove, E. R.; Smith, D. F.; Heeren, R. M. A. *J. Chromatogr., A* **2010**, *1217*, 3946.

(5) Chughtai, K.; Heeren, R. M. A. *Chem. Rev.* **2010**, *110*, 3237.

(6) Meriaux, C.; Franck, J.; Wisztorski, M.; Salzet, M.; Fournier, I. *J. Proteomics* **2010**, *73*, 1204.

(7) Sherrod, S. D.; Diaz, A. J.; Russell, W. K.; Cremer, P. S.; Russell, D. H. *Anal. Chem.* **2008**, *80*, 6796.
(8) Stumpo, K. A.; Russell, D. H. *J. Phys. Chem. C* **2009**, *113*, 1641.
(9) Cha, S.; Song, Z.; Nikolau, B. J.; Yeung, E. S. *Anal. Chem.* **2009**, *81*, 2991.
(10) Tempez, A.; Ugarov, M.; Egan, T.; Schultz, J. A.; Novikov, A.; Della-Negra, S.; Lebeyec, Y.; Pautrat, M.; Caroff, M.; Smentkowski, V. S.; Wang, H.-Y. J.; Jackson, S. N.; Woods, A. S. *J. Proteome Res.* **2005**, *4*, 540.
(11) Sugiura, Y.; Setou, M. *Rapid Commun. Mass Spectrom.* **2009**, *23*, 3269.
(12) Jaskolla, T.; Fuchs, B.; Karas, M.; Schiller, J. *J. Am. Soc. Mass Spectrom.* **2009**, *20*, 867.
(13) Teuber, K.; Schiller, J.; Fuchs, B.; Karas, M.; Jaskolla, T. W. *Chem. Phys. Lipids* **2010**, *163*, 552.
(14) Colsch, B.; Jackson, S. N.; Dutta, S.; Woods, A. S. *ACS Chem. Neurosci.* **2011**, *2*, 213.
(15) Lechene, C.; Hillion, F.; McMahon, G.; Benson, D.; Kleinfold, A. M.; Kampf, J. P.; Distel, D.; Luyten, Y.; Bonventre, J.; Hentschel, D.; Park, K. M.; Ito, S.; Schwartz, M.; Benichou, G.; Slodzian, G. *J. Biol.* **2006**, *5*, 20.1.
(16) Pacholski, M. L.; Cannon, D. M.; Ewing, A. G.; Winograd, N. *Rapid Commun. Mass Spectrom.* **1998**, *12*, 1232.
(17) Bouneau, S.; Brunelle, A.; Della Negra, S.; Depauw, J.; Jacquet, D.; LeBeyec, Y.; Pautrat, M.; Fallavier, M.; Poizat, J. C.; Andersen, H. H. *Phys. Rev. B* **2002**, *65*, 144106.
(18) Touboul, D.; Kollmer, F.; Niehuis, E.; Brunelle, A.; Laprevote, O. *J. Am. Soc. Mass Spectrom.* **2005**, *16*, 1608.
(19) Guillermier, C.; Della Negra, S.; Rickman, R. D.; Pinnick, V.; Schweikert, E. A. *Appl. Surf. Sc.* **2006**, *252*, 6529.
(20) Winograd, N.; Postawa, Z.; Cheng, J.; Skazal, C.; Kozole, J.; Garrison, B. J. *Appl. Surf. Sci.* **2006**, *252*, 6836.
(21) Tempez, A.; Schultz, J. A.; Della-Negra, S.; Depauw, J.; Jacquet, D.; Novikov, A.; Lebeyec, Y.; Pautrat, M.; Caroff, M.; Ugarov, M.; Bensaoula, H.; Gonin, M.; Fuhrer, K.; Woods, A. *Rapid Commun. Mass Spectrom.* **2004**, *18*, 371.
(22) Brunelle, A.; Della-Negra, S.; Deprun, C.; Depauw, J.; Håkansson, P.; Jacquet, D.; le Beyec, Y.; Pautrat, M. *Int. J. Mass Spectrom. Ion Processes* **1997**, *164*, 193.
(23) Pinnick, V. T.; Verkhoturov, S. V.; Kaledin, L.; Bisrat, Y.; Schweikert, E. A. *Anal. Chem.* **2009**, *81*, 7527.
(24) Li, Z.; Verkhoturov, S. V.; Schweikert, E. A. *Anal. Chem.* **2006**, *78*, 7410.
(25) Fernandez-Lima, F. A.; Eller, M. J.; Verkhoturov, S. V.; Della-Negra, S.; Schweikert, E. A. *J. Phys. Chem. Lett.* **2010**, *1*, 3510.
(26) Fletcher, J. S.; Conlan, X. A.; Jones, E. A.; Biddulph, G.; Lockyer, N. P.; Vickerman, J. C. *Anal. Chem.* **2006**, *78*, 1827.
(27) Brunelle, A.; Della-Negra, S.; Depauw, J.; Jacquet, D.; Le Beyec, Y.; Pautrat, M.; Baudin, K.; Andersen, H. H. *Phys. Rev. A* **2001**, *63*, 022902.
(28) Della-Negra, S.; Depauw, J.; Guillermier, C.; Schweikert, E. A. *Surf. Interface Anal.* **2011**, *43*, 62.
(29) Della-Negra, S.; Arianer, J.; Depauw, J.; Verkhoturov, S. V.; Schweikert, E. A. *Surf. Interface Anal.* **2011**, *43*, 66.
(30) Bouneau, S.; Della-Negra, S.; Depauw, J.; Jacquet, D.; Le Beyec, Y.; Mouffron, J. P.; Novikov, A.; Pautrat, M. *Nucl. Instrum. Methods Phys. Res., Sect. B* **2004**, *225*, 579.
(31) Verkhoturov, S. V.; Eller, M. J.; Rickman, R. D.; Della-Negra, S.; Schweikert, E. A. *J. Phys. Chem. C* **2009**, *114*, 5637.
(32) Delvolve, A. M.; Colsch, B.; Woods, A. S. *Anal. Methods* DOI: 10.1039/c1ay05107e.
(33) Jackson, S. N.; Wang, H.-Y. J.; Woods, A. S. *J. Am. Soc. Mass Spectrom.* **2005**, *16*, 2052.
(34) Jackson, S. N.; Ugarov, M.; Egan, T.; Post, J. D.; Langlais, D.; Schultz, J. A.; Woods, A. S. *J. Mass Spectrom.* **2007**, *42*, 1093.
(35) Wehbe, N.; Fallavier, M.; Negra, S. D.; Depauw, J.; Brunelle, A.; Andersen, H. H. *Nucl. Instrum. Methods Phys. Res., Sect. B* **2010**, *268*, 2596.
(36) Novikov, A.; Caroff, M.; Della-Negra, S.; Depauw, J.; Fallavier, M.; Le Beyec, Y.; Pautrat, M.; Schultz, J. A.; Tempez, A.; Woods, A. S. *Rapid Commun. Mass Spectrom.* **2005**, *19*, 1851.
(37) Hager, G. J.; Guillermier, C.; Verkhoturov, S. V.; Schweikert, E. A. *Appl. Surf. Sci.* **2006**, *252*, 6558.
(38) Fernandez-Lima, F. A.; Eller, M. J.; DeBord, J. D.; Verkhoturov, S. V.; Della-Negra, S.; Schweikert, E. A. *Nucl. Instrum. Methods Phys. Res., Sect. B*, accepted for publication.
(39) Jackson, S.; Wang, H.; Woods, A. *J. Am. Soc. Mass Spectrom.* **2007**, *18*, 17.